Journal of
Computational and Theoretical Nanoscience
Vol. 17, 1–6, 2020

Aluminum-Doped Titanium Dioxide Thin Films: A Study of Different Concentrations on Poly(3-hexylthiophene): PhenylC61-Butyric Acid Metheyester-Based Organic Solar Cells

Buraq T. SH. AL-Mosawi[1,*], Mohammed K. Al-Hashimi[1], and Ameer F. Abdulameer[2]

[1] *Dept. of Mathematics, University of Misan, Misan, Iraq*
[2] *Dept. of Physics, College of Science, University of Baghdad, Baghdad, Iraq*

Sol–gel preparation method usually used to prepare the metal oxides. So, it is a rewarding process to prepare the electron selective film made of aluminum-doped titanium dioxide (Al-doped TiO_2). The latter was used to fabricate the inverted organic solar cells P2HT:PCBM. The doping content with Al impact on the optical and morphological characteristics of each film were examined. These characteristics were analyzed depending on the magnified images of the prepared samples by atomic force microscopy (AFM), scanning electron microscopy (SEM), X-ray diffraction (XRD) in addition to the Uv-vis spectroscopic results. The outcomes revealed that the concentration of Al doping has potential influences on the optical properties, XRD results and surface morphology. The *J–V* curve characteristics of each solar cell utilizing Al–TiO_2 film were analyzed and noticed that the most powerful conservation efficiency is 2.09% when using Al–TiO_2 layer with 0.5 wt.% Al as a doping element.

Keywords: Al Doped TiO_2, Organic Solar Cell, P3HT: PCBM, Sol–Gel Method.

RESEARCH ARTICLE

1. INTRODUCTION

Recently, inverted organic solar cell (OSCs) is a piece of attractive equipment to promote the efficiency of OSCs by employing an electrode with larger work function and considerably developed air stability. Interfacial materials with high transparency and conductivity were essential for heterojunction (BHJ) solar cells with effective inversion, which are usually incorporated to connect the conductive electrode and the photoactive layer. Thin layers (10–40) nm were fabricated by the sol–gel method from TiO_2 [1, 2] and ZnO [3–5] where the conventional and inverted OSC uses it as its interfacial layer [6]. Normally, transparency properties of these layers in the visible spectra are high. The active layer was covered by the metal oxide layer to prevent it from oxidation due to high absorption properties in the UV spectra the UV spectra [7, 8]. The charge carrier extraction is improved by using TiO_2 layer in an inverted OSCs structure; the good explanation for this process is the lowering the Fermi energy levels at the cathode electrode [9]. Besides, TiO_2 is used as an electron acceptor layer, which allows the transportation of the charge between poly(3-hexylthiophene) (P3HT) and TiO_2 [3]. There are also several studies show that carrier extraction of the charge and exciton dissociation are affected by TiO_2 and its nano-structured layer [11]. TiO_2 thin film conductivity can be enhanced by increasing the amount of metal ions [12, 13]. Sol–gel preparation method used for doping the TiO_2 films with Al. Sol–gel method is an attractive and widely used method because of its simplicity, possibility to get a larger fabrication area and require low costs in comparison to other methods. $AlCl_3$ and $Al(NO_3)$ are utilized to prepare Al-doped $TiO_2$by sol–gel process and commonly employed as Al dopant ion precursor [14]. The existence of Al as a doping element in thin films structure could foster the states' density (DOS) closer to the Fermi energy level and hence increases the density of the charge carriers that might help in increasing the electrical conductivity [13, 14]. Utilizing the thin film of Al-doped TiO_2 instead of the un-doped TiO_2 layer in solar cells may reduce their impedance which leads to enhance their quality. Moreover, the solar cells performance are unaffected by Al-doped TiO_2 layer thickness variation. This layer has relative higher carrier mobility and concentration of charger carrier compare to the organic one [15].

*Author to whom correspondence should be addressed.

However, based on the authors' knowledge, studying the effect of applying the Al-doped TiO_2 layer on the characteristics of OSCs still under development with limited research outcomes. In the current work, structural, morphological, and optical properties of Al-doped TiO_2 layers with variation of Al concentration were investigated. Besides, the influence of this variation on the OSCs features as an active layer built on hetero-junction of P3HT: PCBM have been demonstrated. The features of these fabricated devices were examined through current density-voltage (J–V) curve with different Al doping content.

2. MATERIALS AND METHODS

2.1. Materials

In the beginning, the materials used in this paper are the titanium isoproposxyde (TIP) (purity: 97%), Au with a purity of 99.99%, [6,6]-phenylC61-butyric acid metheyester (PCBM) and Chlorobenzene solution of poly(3-hexylthiophene) (P3HT). All substances were obtained of Sigma–Aldrich.

2.2. Organic Solar Cell Preparation

The OSCs were prepared by solution processed and thermal evaporation techniques by deposition on glass substrates (ITO). These glass substrates are pre-structured (having a 12 Ω/sq resistivity sheet and the ultrasonic cleans it in alcoholic solution of acetone, isopropyl, and deionized water for ten minutes. Figure 1 describe the structure of the fabricated ORC. Each ORC device consists of four layers TiO_2, P3HT: PCBM blend (active layer), PEDOT: PSS, and Au. TiO_2 layers. Sol–gel method was utilized to manufacture these layers as follows: solvents were made by mixing methanol and isopropanol; then adding titanium isopropoxyde (TIP) (titanium precursor) to the solvent's solution under 80 °C temperature with continuous stirrer. Afterward, the mixture was stirred while the dropping the acetic acid cautiously. TiO_2 layers fabrication procedures are shown in Figure 2. Thin films of

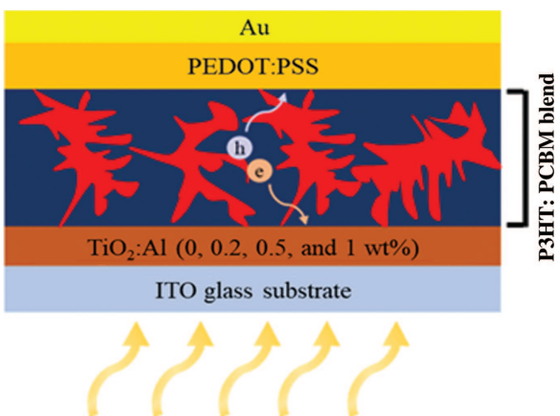

Fig. 1. The structure the fabricated organic solar cell.

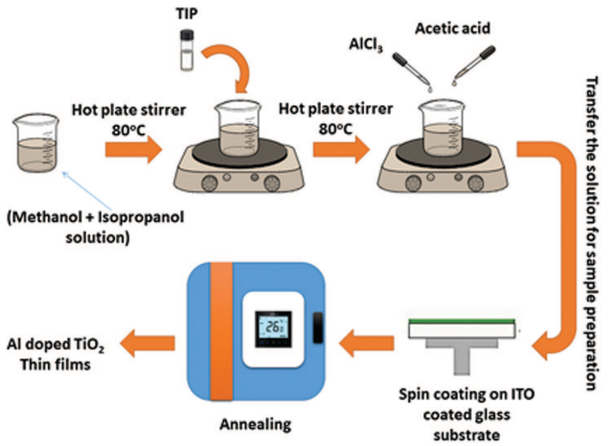

Fig. 2. Steps of preparing TiO_2 thin films.

TiO_2 are spin coated using 2000 rpm spinning speed for 30 sec and then annealed at 600 °C. The thickness of the fabricated TiO_2 thin film was measured as 190 nm using ellipsometry method.

The blend active layers of P3HT: PCBM were prepared by mixing 1:1 ratio of Chlorobenzene solution of P3HT and PCBM [16]. The prepared active layer, then deposited over TiO_2 layer using spin coating process, after that the annealing process was applied at 120 °C on a hot plate in a glove box in the present of nitrogen atmosphere for ten minutes period [17]. The hole transporting layer of poly(3,4 ethylenedioxythiophene): poly(styrene sulfonate) (PEDOT:PSS) is spin coated onto P3HT: PCBM active layer and then thermally treated at 110 °C for ten minutes in the presence of nitrogen atmosphere inside the glove box. Finally, 100 nm thickness of a gold (Au) top contact layer is evaporated thermally by applying 10^{-6} mbar of vacuum and using deposition percent from 0.1–0.2 nm/sec.

3. CHARACTERIZATIONS

The structure and morphology of all thin films of Al-doped TiO_2 were examined using an X'Pert Philips X-ray diffractometer (MPD), scanning electron microscope (FEI-Nova SEM), and nanoscope IIIa multimode AFM (Bruker-AFM). These thin films were optically characterized by UV-visible spectroscopy at 190–1100 nm wavelength range. The thin film thickness parameter was measured by utilizing M200 spectroscopic ellipsometer from J. A. Woollam Company works at 370–1000 nm wavelength. Solar cells are tested electrically (photovoltaic properties) by employing the 4200 Keithley Semiconductor characterization system (SCS). AM 1.5 irradiation of the solar simulator is used to produce intensity of 100 mW/cm^2.

4. RESULTS AND DISCUSSION

The investigation of Al-doped TiO_2 morphology has achieved by the AFM and SEM 3D and 2D-imaging

RESEARCH ARTICLE

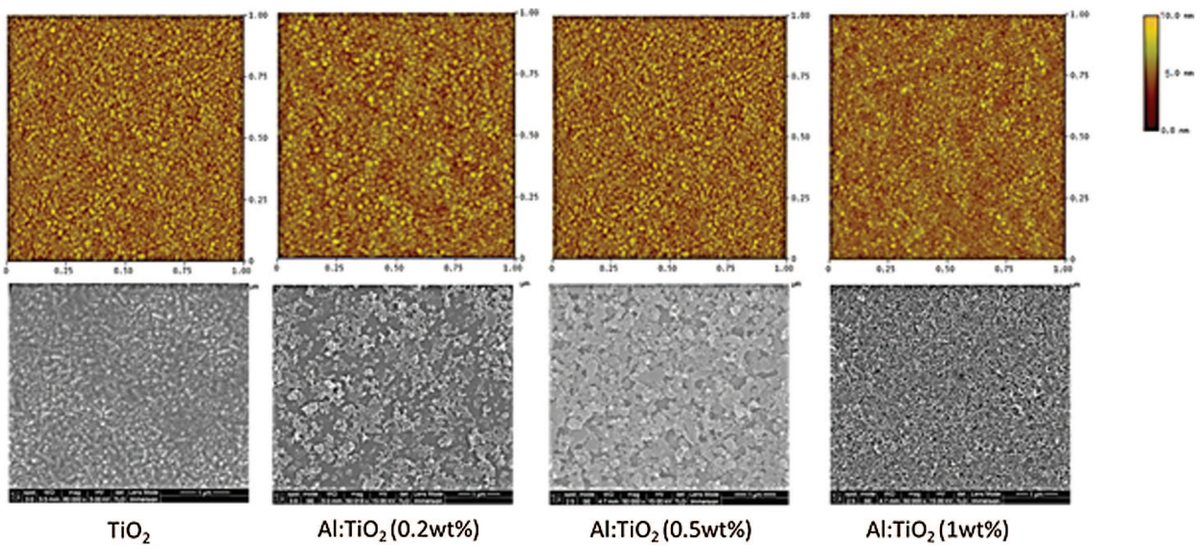

Fig. 3. AFM and SEM micrographs of Al-doped TiO_2 films with various content of Al doping.

systems. Figure 3 displays the SEM and AFM doped and undoped TiO_2 films micrographs with the dissimilar content of the Al doping element. It is found that the concentration of Al doping affects the surface morphology of TiO_2 films. Figure 3 clearly presents that the grain size reduces by increasing the concentration of Al doping which can be attributed to the increasing of bulges' number. Also, the increase of grain packing density in TiO_2 by rising of Al doping concentration may lead to reduce the grain size of TiO_2 [20, 21]. The morphology of the surface of TiO_2:Al (0.5 wt.%) thin film shows a flatter surface with less bulge structures. On the other hand, the film surface images presented by SEM have shown the microstructure form of Al-doped TiO_2, which is consisting of a lot of crystalline particles appeared to be spherical in shape. As well as, the granules uniformly cover the substrate surface. However, Al-doped TiO_2 thin film also demonstrates particles with off-spherical shape. Therefore, doping of Al works to modify the grain look of TiO_2 particles. The microstructure was measured to be regular with compact interconnected grains. Moreover, the doped TiO_2 film shows less porosity than pure TiO_2 film showing that the film becomes denser with incorporation of Al doping [22]. The SEM micrographs prove that the average of the grain size of TiO_2 was decreased by increasing of Al doping [23].

Figure 4 illustrates the X-ray diffraction pattern of each prepared thin film. All samples are polycrystalline with preferential axis orientations (100), (101), (200), (211), (002) and (310). All peaks were identified in the recorded series and attributed to the Rutile TiO_2 phases. The peaks intensity has dropped and the peaks broadening have increased (FWHM) by increasing the Al-doing content. Which means that a deterioration in the crystallization of the thin films has occurred. The growth of TiO_2 grains has endorsed by rapid diffusing of Ti interstitials [24].

When a trivalent cation is used for doping, Ti interstitial content is decreased to compensate the loss of charge, which leads to stop the growth of TiO_2 grains and deteriorating crystallization due to the incorporation of Al into TiO_2 [25]. From AFM micrographs, there is a remarkable difference between crystallite size and the grain size, the latter is much larger size than the crystalline size. While when Al content increased, the grain size decrease, as well crystallite size has changed slightly. Doping of TiO_2 functionally affects the increase of grain size rather on that happened in crystalline size. Such trend relates to the Al-doped TiO_2 inhibition by the $AlCl_3$ [26].

The variation in the optical properties of un-doped and doped TiO_2 with difference Al doping concentrations (0.2,

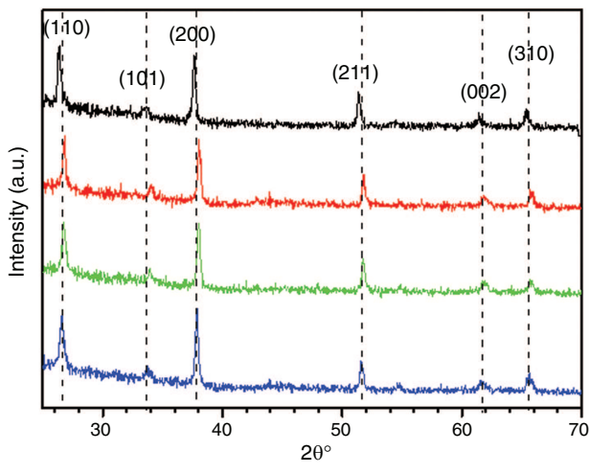

Fig. 4. XRD patterns of TiO_2 films doped with various Al doping concentrations.

RESEARCH ARTICLE

0.5, and 1 wt%) is shown in Figure 5. All the Al-doped TiO_2 films have exhibited high transparent spectra in the visible range (81 to 94%), which is higher than the un-doped TiO_2 film. This can be attributed to Al-doped films absorption transitional nature. The sharp transition in the absorption spectrum occurs for each sample at a wavelength of about 400 nm [27]. The absorption coefficients (α) were calculated for the prepared samples from the optical transmittance measurements depending on the equation below [28]:

$$\alpha = \frac{2.303}{d} \times \log\left(\frac{1}{T}\right) \quad (1)$$

Where d is TiO_2 films thicknesses and T represents the transmittance value.

The equation below represents another method for determining the absorption coefficient of the prepared thin films. This requires the presence of the energy of the incident photon

$$\alpha h\upsilon = A(h\upsilon - E_g)^n \quad (2)$$

Where, h is Planck's constant, υ is the frequency, A is a constant, and n depends on the transition nature. In general, TiO_2 rutile phase associated with the direct transport of the semiconductor bandgap [29]. So that, the direct transition and linear region extrapolation of $(\alpha h\upsilon)^2$ versus $h\upsilon$ curve at $\alpha = 0$ that carries out the direct bandgap of TiO_2 is allowed at transition bandgap of $n = 1/2$ [28]; but, the bandgap transition of $n = 3/2$ is forbidden. Figure 5 illustrates the relation between $(\alpha h\upsilon)^2$ and $h\upsilon$ of each doped TiO_2 film with Al dopant. At higher photon energies, a linear dependence of $(\alpha h\upsilon)^2$ on $h\upsilon$, indicating that the Al-doped TiO_2 films are basically semiconductor with direct transition. The optical band gap (E_{opt}) results from the straight curve part when extrapolating to the zero value. The doped TiO_2 films E_{opt} of different Al-doping concentrations (0, 0.2, 0.5 and 1 wt%), is 3.32 eV, 3.35 eV, 3.37 eV and 3.47 eV, respectively. This band gap broadening can be easily interpreted due to the Moss–Burstein

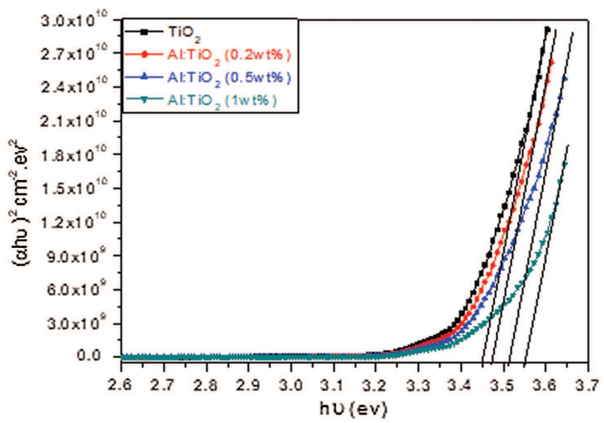

Fig. 5. Plots of $(\alpha h\upsilon)^2$ versus $h\upsilon$ of doped TiO_2 films with various Al doping concentrations.

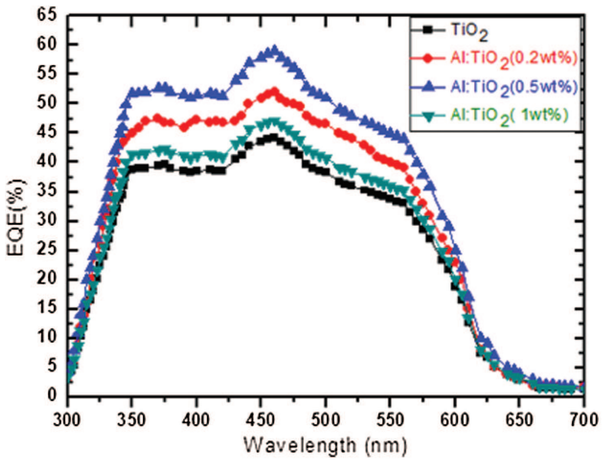

Fig. 6. Effect of Al-doped TiO_2 films with various Al content on the solar cells' spectra (dye-sensitized).

Shift theorem [30]. This is due to the donor electrons occupying shows at the conduction band bottom. Since the Pauli rule keeps states from being doubly occupied and optical transition being vertical, each valence electron requires extra energy into higher levels in the conducting band. Subsequently, the Al-doped TiO_2 E_{opt} films are more broadened than un-doped TiO_2 thin films E_{opt} [30, 31].

Figure 6 shows the action spectra of the solar cells of Al-doped TiO_2 (dye-sensitized) with various Al content. The figure displays that DSSCs based on the Al-doped TiO_2 electrodes showing an important improvement in the incident photon to the current efficiency compared to the un-doped thin film. This development in the efficiency may ascribe to the efficiency improved for injecting an electron and charge-transfer, beside the lightly immense quantity of the absorption of dye as recorded into Table I [32].

The TiO_2 layers incorporated with different Al doping concentration are used to prepare organic solar cells and then were fabricated through ITO/TiO_2: Al/P3HT: PCBM/PEDOT: PSS/Au configuration, as shown perversely in Figure 1. The electrical properties of the manufactured devices were analyzed utilizing J–V curve, as presented within Figure 7. The measurements of J–V curve properties under illuminating with a source of light is achieved for each manufactured organic solar cell with various Al dopants.

Table I. Parameters of OSCs performance evaluated via J–V measurements.

Al-content (wt.%)	Voltage (V_{oc}) (volt)	Current density (J_{sc}) (mA/cm^{-2})	Fill factor (FF)%	Power conversion equipment (PCE)%
0.0	0.59±0.02	4.52±0.3	36±2	0.96
0.2	0.60±0.03	7.61±0.5	41±3	1.87
0.5	0.62±0.02	8.25±0.4	41±3	2.09
1	0.61±0.01	6.02±0.6	30±2	1.10

RESEARCH ARTICLE

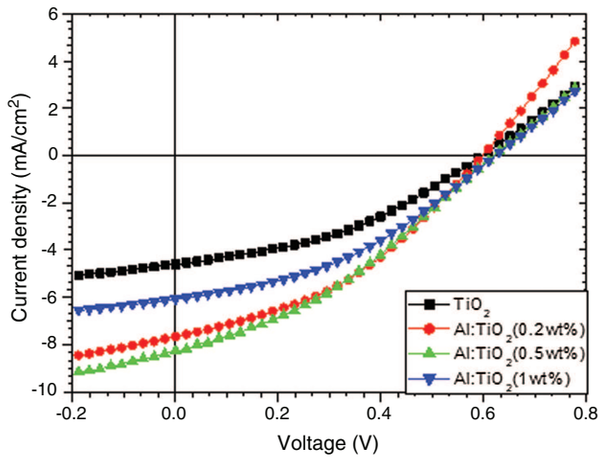

Fig. 7. The J–V characteristics of the OSCs with undoped and doped TiO_2 layers as a function of different Al doping amounts.

From the results, it was found that there was a slight increase in short circuit photocurrent density produced by all of the manufactured solar cells, known as J_{sc} ~4.5–8.25 mA/cm^2. As well, there was a remarkable change in the open circuit voltage indication as he Al dopant varied. The highest voltage was obtained = 0.62 V utilizing doped TiO_2 layer with 0.5 wt% concentration to Al doping. The former variation in the open circuit voltage could be ascribed to the alteration of inherent voltage because of the shifting of Fermi energy level for donor and accepter of doped TiO_2 layer with different Al doping concentration (0, 0.2, 0.5 and 1 wt.%). It is observed that the Fermi level energy will be increase of the energy toward the conduction band of TiO_2 by Al doping, that caused by the shift effect of Burstein–Moss [13, 33, 34]. However, more increasing in Al doping concentration leads to higher charge carrier density, which can explain the increase of the open circuit voltage with increasing in Al doping concentration. Solar cell parameters, such as density of the short circuit current (J_{sc}), open-circuit voltage (V_{oc}), Fill Factor (FF), and Power Conversion Equipment (PCE) are listed in Table I. These parameters were assessed utilizing the Eqs. (3) and (4) below [18]:

$$\mathrm{PCE} = \left(\frac{J_{\max} V_{\max}}{P_{\mathrm{in}}}\right) \tag{3}$$

$$\mathrm{FF} = \frac{J_{\max} V_{\max}}{J_{\mathrm{sc}} V_{\mathrm{oc}}} \tag{4}$$

where J_{sc} is the short circuit current density (mA $\cdot$ cm^{-2}), V_{oc} is the open-circuit voltage (V), J_{max} (mA $\cdot$ cm^{-2}) and V_{max} (V) are the current density and voltage at the point of maximum power output in the J–V curves, and P_{in} is the incident light power [19]. The FF values slightly change with Al doping concentration variation. This behavior could lead to variation of J–V features which may cause by the change of series resistance, and also it could be explained by the variation of the junction features of TiO_2/active layer that is also equivalent to the alignment of the energy level and band bending at the junction. The J–V curve of the solar cell with doped TiO_2 layer with 0.5 wt% Al doping concentration presents the largest area under the J–V curve in comparison to other samples, as shown in Figure 7. This large area attributes to the largest charge carrier extraction [34–36]. The highest PCE is 2.09% which has been obtained for the device of TiO_2 thin film doped with 0.5 wt.% aluminum.

5. CONCLUSIONS

The prepared undoped and doped TiO_2 thin films by different Al content (0.2, 0.5, and 1 wt.%) were fabricated through sol–gel process. Those thin films were studied utilizing AFM, SEM, UV-visible and XRD measurements. Results show that doping of TiO_2 layer with various Al content has an impact on the grain growth, that may result in a variation in the surface morphology. Besides, increasing of Al doping concentration resulted in increasing in the band gap of the fabricated thin films which can attributed to the Moss–Burstein shift. The fabricated organic solar cells with inverted type are structured by utilizing P3HT: PCBM polymer blend and Al-doped TiO_2 layer as their transport layer has conducted. The OSCs were examined by analyzing the J–V curve as a function of Al doping concentration. The behavior of J–V curves shows an enhancement with doped TiO_2 films, compared to undoped film, where the J–V characteristics of solar cell with 0.5 wt.% of Al is better than other Al doping amount. The parameters of solar cell are affected by Al-doped TiO_2 layer. The open voltage is significantly proportional to the concentration of Al-doping for TiO_2 layer that can be attributed to the Fermi energy shifting to higher level in the Al-doped TiO_2 layer. Entirely obtained solar cell properties are notably related to the properties of Al-doped TiO_2 layer, and confirm that doping of TiO_2 layer by Al functionally affects solar cell characteristics.

RESEARCH ARTICLE

Conflict of Interest

The authors declares that no conflict of interest.

References

1. Kim, J.Y., Kim, S.H., Lee, H.H., Lee, K., Ma, W., Gong, X. and Heeger, A.J., **2006**. New architecture for high-efficiency polymer photovoltaic cells using solution-based titanium oxide as an optical spacer. *Advanced Materials*, *18*, pp.572–576.
2. Park, M.H., Li, J.H., Kumar, A., Li, G. and Yang, Y., **2009**. Doping of the metal oxide nanostructure and its influence in organic electronics. *Advanced Functional Materials*, *19*, pp.1241–1246.
3. Yip, H.-L., Hau, S.K., Baek, N.S. and Jen, A.K.Y., **2008**. Polymer solar cells that use self-assembled-monolayer-modified ZnO/metals as cathodes. *Advanced Materials*, *20*, pp.2376–2382.
4. White, M.S., Olson, D.C., Shaheen, S.E., Kopidakis, N. and Ginley, D.S. **2006**. Inverted bulk-heterojunction organic photovoltaic device

using a solution-derived ZnO underlayer. *Applied Physics Letters*, *89*(14), p.143517.
5. Kyaw, A.K.K., Sun, X.W., Jiang, C.Y., Lo, G.Q., Zhao, D.W. and Kwong, D.L., **2008**. An inverted organic solar cell employing a sol–gel derived ZnO electron selective layer and thermal evaporated MoO_3 hole selective layer. *Applied Physics Letters*, *93*, p.221107.
6. Lee, K., Kim, J.Y., Park, H., Kim, S.H., Cho, S. and Heeger, A.J., **2007**. Air-stable polymer electronic devices. *Advanced Materials*, *19*, pp.2445–2449.
7. Esp, N., Dam, H.F., Tan, D.M., Andr, J.W., Jor, M. and Kre, F.C., **2011**. Roll-to-roll processing of inverted polymer solar cells using hydrated vanadium (V) oxide as a PEDOT: PSS replacement. *Materials, 4*, p.169.
8. Hau, S.K., Yip, H.-L., Nam, S.B., Jingyu, Z., Kevin, O. and Alex, J.K.Y., **2008**. Air-stable inverted flexible polymer solar cells using zinc oxide nanoparticles as an electron selective layer. *Applied Physics Letters*, *92*, p.253.
9. Hori, T., Moritou, H., Fukuoka, N., Sakamoto, J., Fujii, A. and Ozaki, M., **2010**. Photovoltaic properties in interpenetrating heterojunction organic solar cells utilizing MoO_3 and ZnO charge transport buffer layers. *Materials*, *3*(11), pp.4915–4921.
10. Peiro, A.M., Rav, P., Gov, K., Boy, D.S., O'Bri, P., Bra, D.C., Nel, J. and Durrant, J.R., **2006**. Hybrid polymer/metal oxide solar cells based on ZnO columnar structures. *Mater. Chem.*, *16*, pp.2088–2096.
11. Wang, K., Wang, S., Xiao, S. and Song, Q., **2018**. Recent advances in Perovskite micro-and nanolasers. *Adv. Opt. Mater., 6*, p.1800278.
12. Jan, A. and Van, C.G., **2009**. Fundamentals of zinc oxide as a semiconductor. *Reports on Progress in Physics*, *72*, p.126501.
13. Imai, Y. and Watanabe, A., **2004**. Comparison of electronic structures of doped ZnS and ZnO calculated by a first-principle pseudopotential method. *Journal of Mater. Sci.: Mater. in Elect.*, *15*, pp.149–156.
14. Hayder, A.H. and Khalid, I.A., **2020**. Effect of dopant concentration in sol–gel derived AZO layer on the efficiency of solar cell with active layer pot: $pc_{71}bm$. *IJPAS*, *7*(1), pp.43–55.
15. Hid, R., Apri, A., Mira, R., Wula, P., Wilk, H.H., Holg, B. and Pari, J., **2011**, *International Symposium on Functional Materials Science*, Bali, April 27th–28th.
16. Kadem, B.Y., Hassan, A.K. and Cranton, W., **2015**. Enhancement of power conversion efficiency of P3HT: PCBM solar cell using solution processed Alq3 film as electron transport layer. *Journal of Mater. Sci.: Mater. in Elect.*, *26*(6), pp.3976–3983.
17. Kadem, B., Hassan, A. and Cranton, W., **2016**. Efficient P3HT: PCBM bulk heterojunction organic solar cells; effect of post deposition thermal treatment. *Journal of Mater. Sci.: Mater. in Elect.*, *27*(7), pp.7038–7048.
18. Yue, G.T., Wu, J.H., Xiao, Y.M., Ye, H.F., Xie, G.X., Lan, Z., Li, Q.H., Huang, M.L. and Lin, J.M., **2010**. Flexible dye-sensitized solar cell based on PCBM/P3HT heterojunction. *Chinese Science Bulletin, 55*, p.835.
19. Kadem, B. and Hassan, A., **2015**. The effect of fullerene derivatives ratio on P3HT-based organic solar cells. *Energy Procedia*, *74*, pp.439–445.
20. Zhang, J.W., He, G., Zhou, L., Chen, H.S., Chen, X.S., Chen, X.F., Deng, B., Lv, J.G. and Sun, Z.Q., **2014**. Microstructure optimization and optical and interfacial properties modulation of sputtering-derived HO_2 thin films by TiO_2 incorporation. *Journal of Alloys and Compounds*, *611*(2014), pp.253–259.
21. Hong, J.L. and Byu-Ok, P., **2003**. Transparent conducting ZnO:Al, in and Sn thin films deposited by the sol–gel method. *Thin Solid Films*, *426*(1–2), pp.94–99.
22. Shreesha, B., Sandeep, K., Prasad, K., Parvathy, M., Sampyady, D. and Bhat, J.S., **2019**. Effect of Al doping on the carrier transport characteristics of TiO_2 thin films anchored on glass substrates. *Applied Physics A, 125*(157), pp.1–7.
23. Bouaine, A., Schmerber, G., Ihiawakrim, D. and Derory, A., **2012**. Structural, optical, and magnetic properties of polycrystalline Co-doped TiO_2 synthesized by solid-state method. *Materials Science and Engineering B, 177*, pp.1618–1622.
24. Kim, S., Kim, M.S., Nam, G. and Leem, J.-Y., **2012**. Structural and blue emission properties of Al-doped ZnO nanorod array thin films grown by hydrothermal method. *Elect. Mate. Lett., 8*, pp.445–450.
25. Fujihara, S., Suzuki, A. and Kimura, T., **2003**. Ga-doping effects on electrical and luminescent properties of ZnO:(La, Eu) OF red phosphor thin films. *Jour. of Appli. Phys., 94*, p.2411.
26. Ji, E.L., Oh, S.-M. and Parka, D.-W., **2004**. Synthesis of nano-sized Al doped TiO_2 powders using thermal plasma. *Thin Solid Films, 457*(1), pp.230–234.
27. Shi, Z., Zhou, M., Zheng, D., Liu, H. and Yao, S., **2013**. Preparation of Ce-doped TiO_2 hollow fibers and their photocatalytic degradation properties for dye compound. *Journal of the Chinese Chemical Society, 60*, pp.1156–1162.
28. Kumarasinghe, P.P.K.K., Dissanayake, A., Pemasiri, B.M.K. and Dassanayake, B.S., **2017**. Thermally evaporated CdTe thin films for solar cell applications: Optimization of physical properties. *Mat. Res. Bull., 96*, pp.188–195.
29. Zhang, J., Zhou, P., Liu, J. and Yu, J., **2014**. New understanding of the difference of photocatalytic activity among anatase, rutile and brookite TiO_2. *Physical Chemist. Chem. Phys.*, *16*(38), p.20382.
30. John, C.I., **1984**. *Many-Body Theory of Solids*. Springer Science & Business Media, p.210.
31. Mousavi, S.H., Muller, T.S. and de Oliveira, P.W., **2013**. Formation and properties of cadmium sulfide buffer layer for CIGS solar cells grown using hot plate bath deposition. *Mater Sci: Mater Electron*, (6), p.3338.
32. Lu, X., Mou, X., Wu, J., Zhang, D., Zhang, L., Huang, F., Xu, F. and Huang, S., **2010**. Improved-performance dye-sensitized solar cells using Nb-doped TiO_2 electrodes: Efficient electron injection and transfer. *Advanced Functional Materials*, *20*, pp.509–515.
33. Bhosle, V., Prater, J.T., Yang, F., Burk, D., Forrest, S.R. and Narayan, J., **2007**. Gallium-doped zinc oxide films as transparent electrodes for organic solar cell applications. *Jour. of Appl. Phys.*, *102*, pp.023501–023505.
34. Kar, J.P., Kim, S., Shin, B., Park, K.I., Ahn, K.J., Lee, W., Cho, J.H. and Myoung, J.M., **2010**. Influence of sputtering pressure on morphological, mechanical and electrical properties of Al-doped ZnO films. *Solid-State Electronics*, *54*, p.1447.
35. Barsoukov, E. and Macdonald, J.R., eds., **2007**. *A Review of: Impedance Spectroscopy, Theory, Experiment, and Applications*. Wiley-Interscience, John Wiley & Sons, Inc.
36. Conings, B., Baeten, L., Boyen, H., Spoltore, D., D'Haen, J., Grieten, L., Wagner, P., Van bael, M.K. and Manca, J.V., **2012**. Relation between morphology and recombination kinetics in nanostructured hybrid solar cells. *The Journal of Physical Chemistry C*, *116*(27), pp.14237–14242.

Received: 13 August 2020. Accepted: 28 August 2020.

RESEARCH ARTICLE